TRAVELING WAVE PARAMETRIC AMPLIFIER WITH JOSEPHSON JUNCTIONS USING MINIMAL RESONATOR PHASE MATCHING (SUPPLEMENTARY INFORMATION)

Coupled Mode Equations

A circuit diagram of a Josephson junction embedded nonlinear transmission line is shown in Fig. 1(a) in the main text. The Josephson inductance is current dependent,

$$L(I) = L_0 \left[1 + \frac{1}{2} \frac{I^2}{I_c^2} \right], L_0 = \frac{\Phi_0}{2\pi I_c} \tag{S1}$$

where Φ_0 is the magnetic flux quantum and I_c is the critical current of the Josephson junction. Consequently, propagation along the transmission line is described by a nonlinear wave equation:

$$\frac{\partial^2 I}{\partial z^2} - \frac{1}{\tilde{c}^2} \frac{\partial^2}{\partial t^2} \left[I + \frac{1}{6} \frac{I^3}{I_c^2} \right] = 0, \ \frac{1}{\tilde{c}^2} \approx LC, \tag{S2}$$

Eqn. S2 is analogous to the case of light traveling in nonlinear Kerr media, in which the index of refraction is intensity-dependent. The propagation can be solved using the coupled-mode equations (CME) method from nonlinear optics. [1]

We write the pump, signal and idler as $I = 1/2 \left[\sum_n A_n e^{i(k_n z - \omega_n t)} + c.c. \right]$ where A_p, A_s and A_i represent the three traveling waves of pump, signal and idler, respectively. Following the CME approach, we derive the coupled-mode equations under the slow wave approximation (SWA), [2] [3]

$$\frac{dA_p}{dz} = \frac{ik_p}{16I_c^2} A_p |A_p|^2$$

$$\frac{dA_s}{dz} = \frac{ik_s}{16I_c^2} \left(2A_s |A_p|^2 + A_i^* A_p^2 e^{-i\Delta kz} \right)$$

$$\frac{dA_i}{dz} = \frac{ik_i}{16I_c^2} \left(2A_i |A_p|^2 + A_s^* A_p^2 e^{-i\Delta kz} \right), \tag{S3}$$

where $\Delta k = k_i + k_s - 2k_p$ is the phase mismatch calculated from weak-signal dispersion of the transmission line. The term on the right hand side of the pump equation represents the self-phase modulation due to the AC pump current interacting with itself. Analogous cross-phase modulation processes are represented by the first term on the right hand side of the signal and idler equations; the other term presents the conversion of two pump photons to a signal

photon and an idler photon. Under the undepleted pump assumption $|A_p| \gg |A_i|, |A_s|$, the pump can be solved first

$$A_p = A_p(0)e^{i\gamma k_p z}, \gamma = \frac{|A_p(0)|^2}{16 I_c^2}, \tag{S4}$$

where γ is an unit-less coefficient reflecting the strength of the nonlinear effect and $\phi_{nl} = \gamma k_p z$ is the nonlinear phase shift of the pump also referred to as the self phase modulation (SPM) in nonlinear optics. Using the pump solution, the signal and idler can be solved perturbatively. Here, we write the solution in a matrix form,

$$\begin{bmatrix} A_s(z) \\ A_i^*(z) \end{bmatrix} = M(z, A_p(0)) \begin{bmatrix} A_s(0) \\ A_i^*(0) \end{bmatrix}, \quad M = \begin{bmatrix} u_{11} & u_{12} \\ u_{21} & u_{22} \end{bmatrix}$$

$$u_{11} = \left[\cosh(gz) + i\frac{\kappa}{2g}\sinh(gz) \right] e^{i(2\gamma k_s - \frac{\kappa}{2})z},$$

$$u_{12} = \left[\frac{i\gamma k_s}{g} e^{2i\phi_0} \sinh(gz) \right] e^{i(2\gamma k_s - \frac{\kappa}{2})z},$$

$$u_{21} = \left[-\frac{i\gamma k_i}{g} e^{-2i\phi_0} \sinh(gz) \right] e^{-i(2\gamma k_i - \frac{\kappa}{2})z},$$

$$u_{22} = \left[\cosh(gz) - i\frac{\kappa}{2g}\sinh(gz) \right] e^{-i(2\gamma k_i - \frac{\kappa}{2})z},$$

$$e^{i\phi_0} = \frac{A_{p0}}{|A_{p0}|}, \quad g = \sqrt{\left(\frac{k_s k_i}{k_p^2} \right)(\gamma k_p)^2 - \left(\frac{\kappa}{2} \right)^2}, \quad \kappa = 2\gamma k_p + \Delta k. \tag{S5}$$

If the transmission line has no intrinsic dispersion ($\Delta k = 0$, as is our case for the junction embedded transmission line in the low frequency limit), it can be derived from Eqn. S5 that the maximum signal gain (occurring at $\omega_s = \omega_p$) is quadratic in ϕ_{nl} or z (thus the length of the line)[4, 5] ,

$$g \to 0, \quad u_{11} = (1 + i\gamma k_p z)e^{i\gamma k_p z}, \quad G_q = |u_{11}|^2 = 1 + \phi_{nl}^2. \tag{S6}$$

If additional dispersion $\Delta k = -2\gamma k_p$ is introduced (as is the case in the dispersion engineered kinetic inductance parametric amplifier [2]) so that the phase matching condition is perfectly met ($\kappa = 0$), exponential signal gain can be achieved,

$$G_e = \cosh^2(\phi_{nl}) \approx \exp(2\phi_{nl})/4. \tag{S7}$$

Resonantly Phase-matched TWPA

Assume that N - 1 phase shifters (resonators) are inserted in between N sections of dispersionless line at position z_m (see Figure S1). We treat the resonators as perfect phase
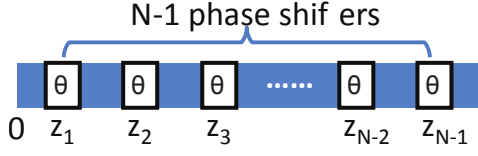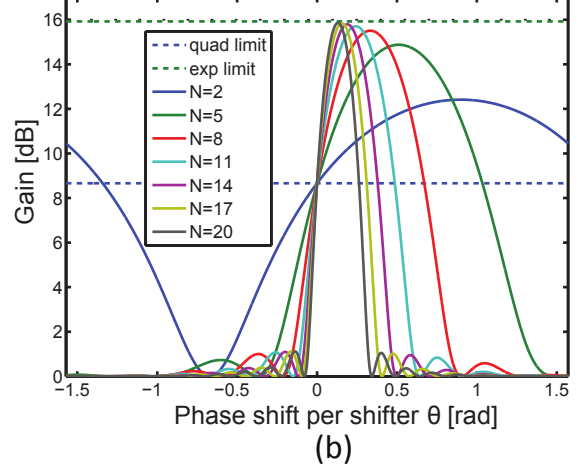
Figure S1. (a) Configuration of $N-1$ phase shifters inserted between N nonlinear transmission line sections. (b) Comparison of enhanced gain with the quadratic gain and exponential gain limits. $\phi_{nl} = 2.5$ is assumed which corresponds to our device.

.

shifters for which $S_{21} = 1$ at all frequencies except the pump, where we have $S_{21}(\omega_p) = e^{i\theta}$. The output signal/idler at z_N and the total signal gain can be calculated by cascading the M matrices

$$\begin{bmatrix} A_s(z_N) \\ A_i^*(z_N) \end{bmatrix} = M(z_N - z_{N-1}, \ A_p(z_{N-1}^+))M(z_{N-1} - z_{N-2}, \ A_p(z_{N-2}^+))...M(z_1, \ A_p(0)) \begin{bmatrix} A_s(0) \\ A_i^*(0) \end{bmatrix}$$

$$= \hat{M}(z_N, A_p(0)) \begin{bmatrix} A_s(0) \\ A_i^*(0) \end{bmatrix}, \ G_r = |\hat{M}_{11}|^2. \tag{S8}$$

where $A_p(z_m^+)$ has included the additional phase shift θ from the phase shifter at z_m and $\hat{M}$ is the cumulative transfer matrix for signal/idler from $z = 0$ to $z = z_N$. A Matlab program is written to compute $\hat{M}$ and G_r. We are mostly interested in the dependence of G_r on the number of phase shifters N and the phase shift per shifter θ. Fig. S1 (b) shows the calculation results, using the realistic design parameters of the device. It is clear that the gain is greatly enhanced by the phase shifters, even when only 1 phase shifter ($N = 2$) is inserted. The enhancement increases with N and approaches the exponential gain limit for large N. In fact, the enhanced gain is very close to G_e limit (green dashed line) for 7 or more phase shifters ($N > 8$). Adding resonators per unit LC ladder was recently proposed in [6] to achieve phase matching condition.
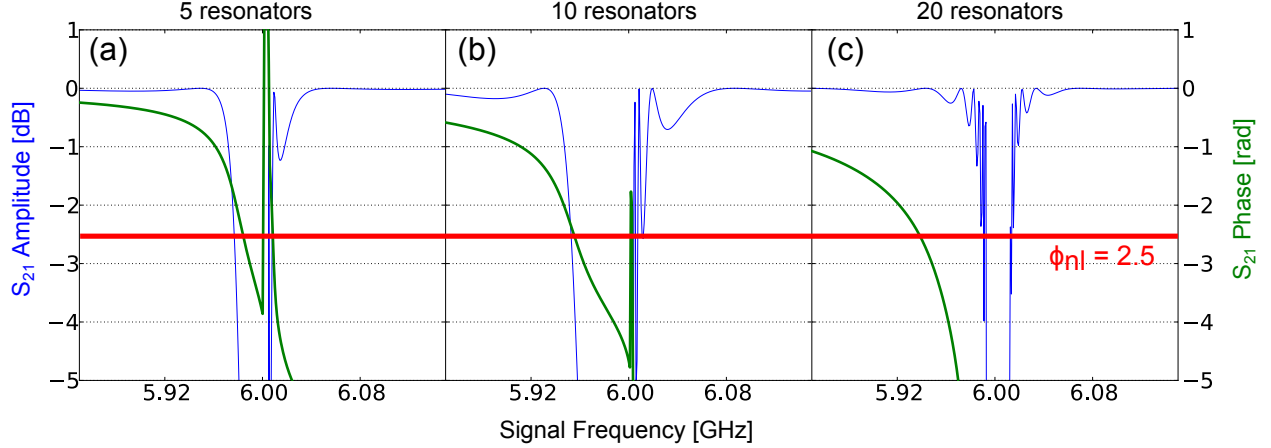
Figure S2. Plots showing simulated signal phase and amplitude vs frequency for (a) 5 resonators, (b) 10 resonators, or (c) 20 resonators in a TWPA circuit. The plots show that while only a few ideal phase shifters are necessary for phase matching, $\lambda/4$ resonators also cause an amplitude dip which can affect pump transmission close to resonance. Adding additional resonators allows for a greater phase shift with a smaller reflected pump amplitude. The red line indicates a nonlinear phase shift of 2.5 radians which is necessary to achieve gain greater than 15 dB.

.

An ideal phase shifter can be approximated by a $\lambda/4$ resonator capacitively coupled to the transmission line. The resonator provides a frequency dependent phase shift as well as an amplitude dip which is maximized on resonance. With only a few resonators 5-10, it is impossible to achieve the desired phase shift without tuning the pump into the amplitude dip of the resonator. This will destroy the parametric gain through internal reflections in the transmission line. To ensure we can achieve the desired phase shift with virtually no affect on pump amplitude we must use a design with $N \geq 20$. The dependence of phase and amplitude on frequency is shown for several numbers of resonators in Fig. S2. As these simulations were only meant to determine phase shift vs amplitude dip, they do not include the possibility of an additional phase shift coming from the periodic placement of resonators. The simulated phase shift shown in Fig. 3(c) of the main text includes this effect and better reflects experimental conditions.

4

TWPA Device Parameters

Constructing the nonlinear sections of the TWPA requires balancing between the critical current of the Josephson junctions and the cutoff frequency of the LC ladder. If the critical current is increased it will require a larger pump to achieve the same nonlinearity. Saturation power depends directly on pump amplitude so a higher critical current for each junction is desirable. However higher critical current also means a lower inductance per section in the LC ladder which means a higher cutoff frequency given by $1/(2\pi\sqrt{L_{sec}C_{sec}})$. A lower cutoff frequency is desirable because it will prevent parasitic coupling of the pump to higher frequency modes[7]. Thus we constructed each section with three higher critical current junctions in a row, such that $L_{sec} = 3L_j$. This allowed us to use higher critical current junction while also lowering the cutoff frequency of the transmission line by a factor of three. The capacitance was then increased to maintain $\sqrt{\mathcal{L}/\mathcal{C}} \approx 50\,\Omega$ given inductance per unit length $\mathcal{L}$ and capacitance per unit length $\mathcal{C}$

As stated in the main text the critical current of each junction was designed to be $\approx 5\,\mu$A which corresponds to an inductance of $65\,$pH and a section inductance of $195\,$pH. The capacitance of each parallel plate capacitor was designed to be 117 fF leading to a cutoff frequency of $33\,$GHz. This cutoff frequency combined with the dispersion engineering is sufficient to prevent the propagation of shock-waves in the transmission line[7]. The geometric inductance and capacitance per unit length were extracted from simulations matching the nonlinear transmission line geometry. Combining the simulation data with the single section values give $\mathcal{L} = 3.5\,\mu$H/m and $\mathcal{C} = 1.5\,$nF/m for a combined impedance of $\approx 48\,\Omega$. The impedance was designed to be less than $50\,\Omega$ initially as impedance will increase slightly when in operation do to the nonlinear inductance.

The resonators were initially designed to operate at a frequency of $7\,$GHz but shifted lower in frequency to $6.1\,$GHz due to kinetic inductance in the thin $60\,$nm aluminum film. Resonators being placed at the end of each nonlinear section means they are $1100\,\mu$m apart. The propagation velocity coming from the inductance and capacitance per unit length means $1100\,\mu$m corresponds to $\lambda/2$ for $6.2\,$GHz. This is consistent with what we observe experimentally.
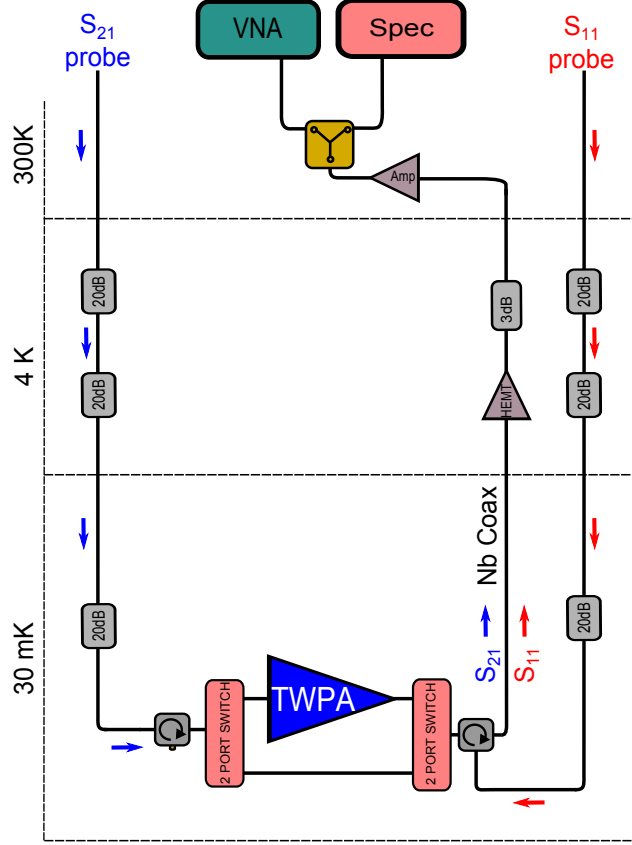
Figure S3. Diagram of the transmission measurement experiment used to characterize TWPA transmission and reflection amplitudes. The output port of a vector network analyzer (VNA) can be attached to either port and combined with the TWPA pump. The signal output is then split at room temperature between the VNA and a spectrum analyzer (SPEC) used for noise measurements. This setup allows us to probe both S_{21} and S_{11} in a single cool down of the refrigerator using equivalent measurement paths.

Measuring TWPA Transmission

For the TWPA to function as an effective amplifier it must first function as a transmission line. If the individual sections are not well impedance matched, internal reflections can destroy the coupling between different frequency modes. Excessive loss in the line can become a source of noise which will make quantum-limited amplification impossible. To check the transmission line behavior of the TWPA we measured its transmission (S_{21}) and reflection (S_{11}) amplitude compared to that of a standard low loss microwave cable. This experiment was carried out using two 2-port cryogenic microwave switches as well as two
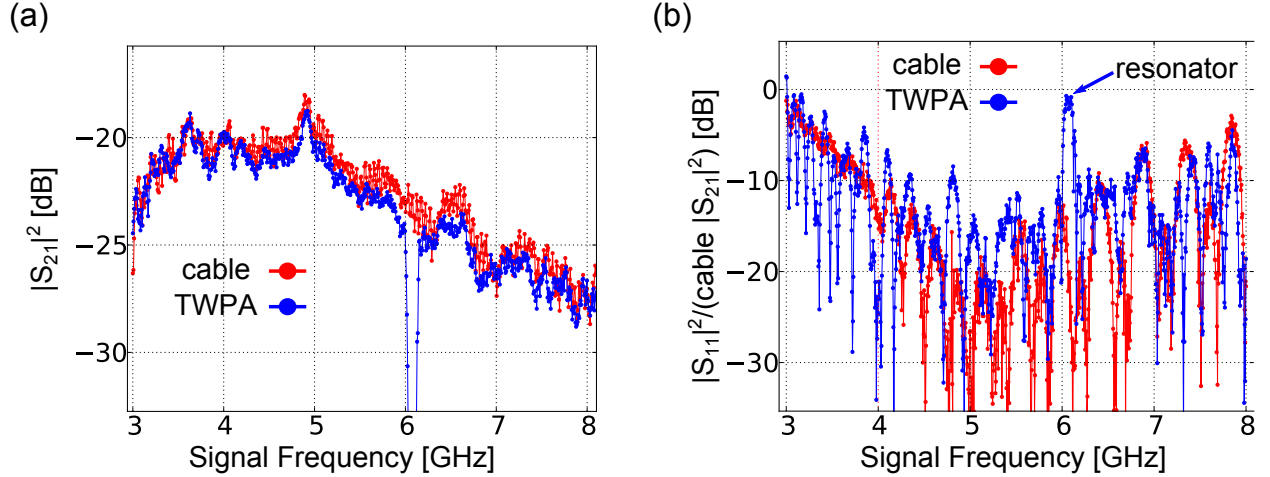
Figure S4. (a) Measured transmission amplitude of both a low loss microwave cable (red) and the TWPA (blue). The TWPA shows a slight decrease in transmission over the range but the deviation is only 0.5 dB. (b) Measurement of reflection amplitude of the cable (red) and the TWPA (blue) scaled relative to the cable transmission from (a). The TWPA's higher reflection amplitude is consistent in magnitude with the lower transmission from part (a), which indicates the majority of the difference comes from reflection in the TWPA rather than loss in the materials.

cryogenic microwave circulators, shown in Fig. S3. The switches were used to swap the TWPA and cable in the transmission path to the high electron mobility transistor (HEMT) amplifier. Two equivalent microwave inputs were used to probe the transmission and reflection simultaneously. The S_{21} probe line goes through the first circulator, the TWPA, and finally the last circulator, before going to the HEMT. The S_{11} line goes to the third input of the last circulator which funnels it to the opposite end of the TWPA. Any reflected signal then makes its way to the HEMT.

The data from this experiment is shown in Fig. S4. Figure S4 (a) shows that the TWPA and cable have the same transmission profile over the majority of the bandwidth. There is an average decrease in transmission of 0.5 dB relative to a copper cable, except at the resonator frequency (6.1 GHz) where there is a significant amplitude dip. The S_{21} data for both devices is shown in Fig. S4 (b) with both data sets scaled relative to S_{21} for the cable. The TWPA reflection is in general less than -10 dB relative to the cable transmission, which is consistent with -0.5 dB less transmission. These two data sets taken together suggest that any drop in transmission through the TWPA comes from reflections rather than loss in the transmission line.
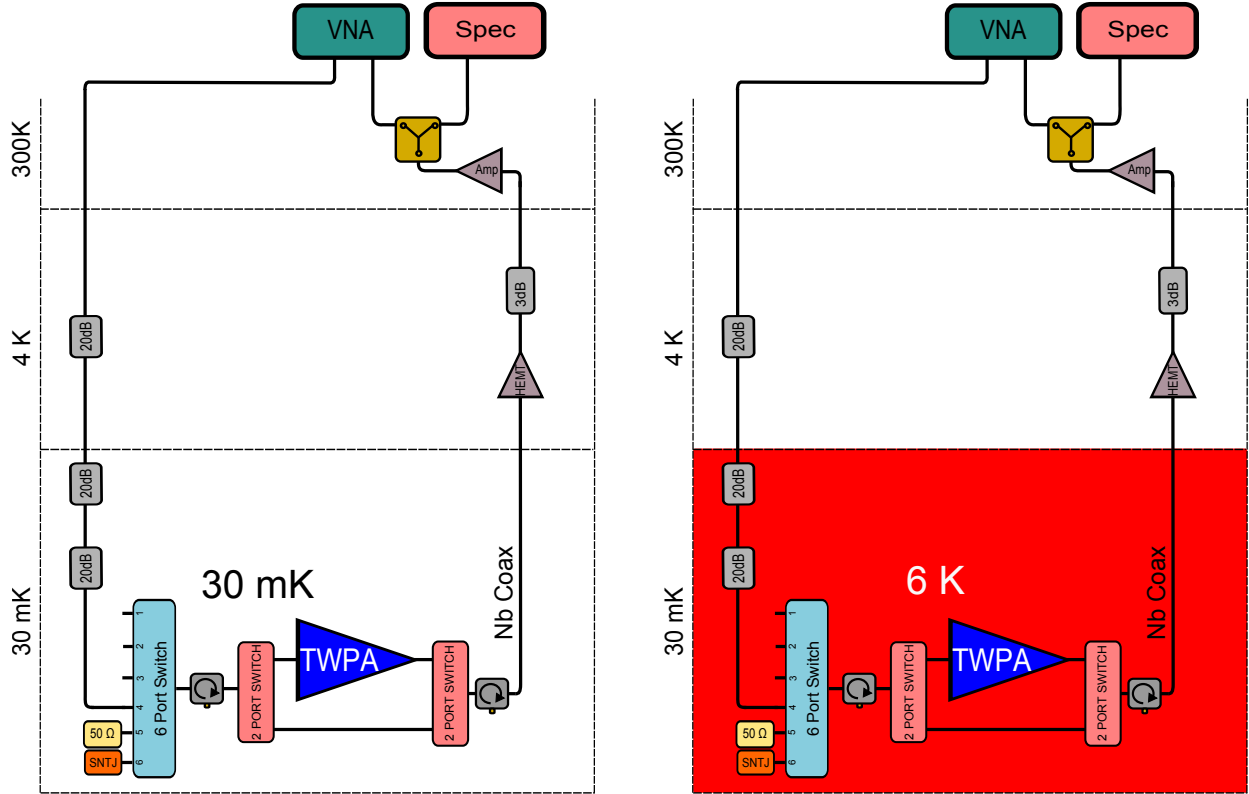
Figure S5. Schematic for paramp experimental setup used to characterize noise. The left figure shows the experimental setup with paramp, circulators, and microwave switches at base temperature. The $50\,\Omega$ on the 6 port switch is heated to calibrate the HEMT noise. The right schematic shows the portion of the fridge heated (red) to perform a y-factor measurement. When this calibration is done the 2 port switches are are set to the straight through path which provides 2 circulator channels between the $50\,\Omega$ and the HEMT, in constrast to the TWPA which is separated from the HEMT by just one circulator. As circulators are the dominant source of loss, the HEMT system noise seen by the paramp and the $50\,\Omega$ should only differ by 0.5-1 dB. This however would skew the system noise higher so it should at least provide an upper bound to the TWPA added noise.

Characterizing Noise temperature

The TWPA system noise values displayed in this paper were calculated using the method of signal to noise ratio improvement [8, 9] discussed in the main text. In this method the amplified noise and transmission amplitude is first measured when the amplifier is turned off. The amplifier is then turned on and the amplified noise and transmission amplitude are once again measured. By comparing the increase in transmission power (gain) to the increase in

amplified noise we can measure system noise amplified by the TWPA, provided we know the system noise amplified by the HEMT. In this measurement signal loss between the TWPA and the HEMT can make this ratio seem smaller and must be taken into account when measuring the amplified HEMT noise. In our setup, shown in Fig. S5, we use a y-factor measurement [10] with a heated $50\,\Omega$ NiCr resistor on the cold plate of our refrigerator. In this setup both the TWPA is switched out of the line leaving a $50\,\Omega$ resistor connected to the HEMT by low loss copper microwave flex cables at $30\,$mK, 1-2 circulators, and a Nb coaxial cable connected between $30\,$mK and the HEMT at $4\,$K. Due to the difficulty of heating just the $50\,\Omega$ resistor we use a method in which the entire cold plate of the refrigerator in heated to a much larger temperature ($6\,$K) and allowed to stabilize before a measurement is performed. The HEMT amplifier is on a different plate and its temperature is held steady over the course of this experiment. This methodology, while allowing for accurate temperature measurement of the resistor, can mis-characterize the effect of loss between the resistor and the HEMT. Any dissipative loss coming from attenuation on the $30\,$mK plate would add noise to the signal as it was also at the higher $6\,$K temperature. We assume the dominant source of potential loss comes from the microwave circulators, as the superconducting and copper cables should have negligible loss at these temperatures. The circulator insertion loss was measured at room temperature to be between 0.5 and $1\,$dB. To account for this we have added $1\,$dB error bars to our measurement of the HEMT noise which are in turned scaled to give error bars for the signal to noise ratio improvement of the TWPA. A second complication arises from the small gain of the TWPA in this experiment. We were unable to achieve the high 12-14 dB gain displayed earlier in the noise characterization experiment. Rather the SNR improvement was measured with an average gain of 6-8 dB. At this level the TWPA gain is not enough to overcome the added noise of the HEMT at 4K. Thus the lowest system noise we achieve is between 600-700 mK or 2 photons. After accounting for the residual HEMT noise these numbers are consistent with a single photon of amplified quantum noise.

[1] G. P. Agrawal, *Nonlinear fiber optics* (Academic press, 2007).

[2] B. H. Eom, P. K. Day, H. G. LeDuc, and J. Zmuidzinas, Nat. Phys. (2012).

[3] S. Chaudhuri, K. Irwin, and J. Gao, arXiv preprint arXiv:1412.2372 (2014).

[4] O. Yaakobi, L. Friedland, C. Macklin, and I. Siddiqi, Phys. Rev. B **87**, 144301 (2013).

[5] S. Chaudhuri and J. Gao, arXiv preprint arXiv:1308.2951 (2013).

[6] K. O'Brien, C. Macklin, I. Siddiqi, and X. Zhang, Phys. Rev. Lett. **113**, 157001 (2014).

[7] R. Landauer, IBM Journal of Research and Development **4**, 391 (1960).

[8] M. Hatridge, R. Vijay, D. Slichter, J. Clarke, and I. Siddiqi, Phys. Rev. B **83**, 134501 (2011).

[9] J. Mutus, T. White, E. Jeffrey, D. Sank, R. Barends, J. Bochmann, Y. Chen, Z. Chen, B. Chiaro, A. Dunsworth, et al., Appl. Phys. Lett. **103**, 122602 (2013).

[10] D. M. Pozar, *Microwave engineering* (John Wiley & Sons, 2009).